

# Excess Ferrous Iron Promotes the Construction of Extracellular Electron Pathways in the Iron-corroding Bacterium *Desulfovibrio ferrophilus* IS5

Xiao DENG,<sup>1)\*</sup> Jun KIKKAWA<sup>2)</sup> and Akihiro OKAMOTO<sup>1,3,4,5)</sup>

1) Research Center for Macromolecules and Biomaterials, National Institute for Materials Science, 1-1 Namiki, Tsukuba, Ibaraki, 305-0044 Japan.

2) Center for Basic Research on Materials, National Institute for Materials Science, 1-1 Namiki, Tsukuba, Ibaraki, 305-0044 Japan.

3) Graduate School of Chemical Sciences and Engineering, Hokkaido University, Kita 13, Nishi 8, Kita-ku, Sapporo, 060-8628 Japan.

4) Graduate School of Science and Technology, University of Tsukuba, 1-1-1 Tennodai, Tsukuba, 305-8577 Japan.

5) Research Center for Autonomous Systems Materialogy, Institute of Science Tokyo, 4259 Nagatsuta-cho, Midori-ku, Yokohama, Kanagawa, 226-8501 Japan.

(Received October 24, 2025; Accepted February 5, 2026; Advance online published February 18, 2026;  
Published April 15, 2026)

Microbial extracellular electron uptake (EEU) is central to bioelectrochemical processes and biocorrosion, yet its underlying mechanisms are not fully understood under microbially influenced iron corrosion. Here, we investigate how excess  $\text{Fe}^{2+}$  modulates EEU in *Desulfovibrio ferrophilus* IS5, a strain that causes severe anaerobic iron corrosion via outer-membrane cytochromes (OMCs)-mediated electron uptake. We show that IS5 grown with elevated  $\text{Fe}^{2+}$  exhibits substantially enhanced EEU. This enhancement arises through two complementary mechanisms: (i) increased abundance of functional OMCs via the upregulation of a cytochrome assembly protein, and (ii) an additional electron transfer route mediated by FeS nanoparticles precipitated on the IS5 outer membrane. This indicates that, during iron corrosion, when IS5 cells are found within thick layers of corrosion products and biofilms, they simultaneously utilize both OMCs and FeS nanoparticles to sustain high-rate EEU from iron under conditions of high  $\text{Fe}^{2+}$  concentrations and limited organic substrates. This study advances the mechanistic understanding of EEU-driven iron corrosion and highlights a potential avenue for manipulating bioelectrochemical systems.

KEY WORDS: microbially influenced corrosion; sulfate-reducing bacteria; iron sulfide nanoparticles; outer-membrane cytochrome; electrochemical analyses; transmission electron microscopy; transcriptome.

## 1. Introduction

The anaerobic corrosion of iron, which occurs in buried pipelines and storage tanks, presents serious challenges to energy infrastructure and results in enormous economic losses, estimated at hundreds of billions of dollars annually.<sup>1,2)</sup> This type of corrosion is largely accelerated by microbial metabolic activity, particularly that of sulfate-reducing bacteria (SRB),<sup>3,4)</sup> and is therefore termed microbially influenced corrosion (MIC). SRB produce corrosive hydrogen sulfide and consume hydrogen that accumulates on the iron to accelerate anaerobic iron dissolution.<sup>5)</sup> In addition, certain sediment-derived SRB, including

*Desulfovibrio ferrophilus* IS5, are proposed to corrode iron through direct extracellular electron uptake (EEU).<sup>6)</sup> These SRB exhibit distinct corrosion capabilities compared to conventional SRB—they can grow using iron granules as the sole electron donor and can continuously corrode iron at high rates on thick, electrically conductive corrosion crusts.<sup>7)</sup> This indicates that microbial electron uptake-driven corrosion poses especially severe threats and high risks.<sup>8)</sup> Therefore, understanding the EEU mechanism in SRB has become a key focus in the MIC field.

Given that the bacterial outer membrane (OM) represents the barrier for EEU from solids, identifying electron conduits spanning the OM is crucial. Two pathways have been described in SRB: outer-membrane cytochromes (OMCs) containing multi-heme redox centers,<sup>9)</sup> and electrically con-

\* Corresponding author: E-mail: deng.xiao@nims.go.jp



ductive iron sulfide (FeS) nanoparticles biosynthesized on the OM.<sup>10</sup> For instance, *D. ferrophilus* IS5, when deprived of soluble organic electron donors, produces OMCs to mediate EEU from electrodes,<sup>9</sup> whereas *D. vulgaris* Hildenborough, which does not possess OMCs, makes use of FeS nanoparticles deposited on its OM to facilitate EEU.<sup>10</sup>

Although IS5 may precipitate FeS nanoparticles on its OM through the reaction of sulfide with iron ions bound to the negatively charged cell surface,<sup>11</sup> this potential EEU route has not been tested. Notably, previous transmission electron microscopy (TEM) of IS5 cross-sections revealed the cell surface densely covered with OMCs but no obvious OM-associated FeS nanoparticles.<sup>9</sup> This absence can be attributed to the low Fe<sup>2+</sup> concentration (7.6  $\mu$ M) in the growth medium, which was sufficient for heme synthesis but inadequate for substantial FeS precipitation, a process that typically requires millimolar iron levels.<sup>11,12</sup> Such millimolar concentrations, however, are common during active MIC.<sup>13</sup> Thus, a comprehensive understanding of IS5 corrosion requires investigating how high iron availability affects EEU.

This study examines how high-iron growth conditions influence the establishment of EEU pathways in IS5, focusing on OMCs expression and the potential formation of OM-associated FeS nanoparticles as an additional electron uptake route.

## 2. Experimental Conditions

### 2.1. Cultivation of IS5

*Desulfovibrio ferrophilus* IS5 was precultivated for 3 days in 60 mL of DSMZ medium 195c<sup>14</sup> in 100 mL glass vials at 28°C under an anoxic headspace of CO<sub>2</sub>/N<sub>2</sub> (20:80, v/v). An inoculum of 2% (v/v) was transferred to 60 mL of DSMZ medium 195c (containing 7.6  $\mu$ M Fe<sup>2+</sup>) or an Fe<sup>2+</sup>-enriched artificial seawater (EASW) medium (containing 3.6 mM Fe<sup>2+</sup>) previously reported.<sup>15</sup> The EASW contained (g/L): NaCl 23.5, Na<sub>2</sub>SO<sub>4</sub> 3.9, NaHCO<sub>3</sub> 0.2, MgCl<sub>2</sub> 5.0, CaCl<sub>2</sub>×2H<sub>2</sub>O 1.5, CaSO<sub>4</sub>×2H<sub>2</sub>O 0.1, SrCl<sub>2</sub>×6H<sub>2</sub>O 0.04, KCl 0.7, KBr 0.1, H<sub>3</sub>BO<sub>3</sub> 0.03, trisodium citrate 0.5, sodium lactate 3.5, yeast extract 1.0, NH<sub>4</sub>Cl 0.1, MgSO<sub>4</sub>×7H<sub>2</sub>O 0.7, Fe(NH<sub>4</sub>)<sub>2</sub>(SO<sub>4</sub>)<sub>2</sub>×6H<sub>2</sub>O 1.4, K<sub>2</sub>HPO<sub>4</sub> 0.05, L-cysteine 0.1. For further cultivation, an inoculum of 2% (v/v) was transferred into fresh medium and grown for an additional four days.

### 2.2. TEM

IS5 cells grown for 4 days in DSMZ medium 195c or EASW medium were harvested by centrifugation at 7 800 × g for 10 min and immediately fixed in precooled fixation solution (2.5% glutaraldehyde and 4% paraformaldehyde prepared in phosphate buffer) for 12 h at 4°C in the dark without agitation. The cells were then washed five times with sodium-HEPES buffer (50 mM, pH 7.4, containing 35 g/L NaCl). The pellet was dehydrated through an ethanol gradient (25%, 50%, 75%, and 100%, 10 min each) with gentle rotation, followed by centrifugation at 10 000 × g for 5 min. The 100% ethanol wash was repeated three times. Dehydrated cells were infiltrated with 50% LR White resin (prepared in 100% ethanol) for 30 min at 4°C with gentle rotation, then centrifuged (6 000 × g, 5 min). The pellet was subsequently incubated in 100% LR White

resin for 60 min at 4°C with rotation, centrifuged again (6 000 × g, 5 min), and the resin was replaced with fresh 100% LR White. Polymerization was carried out at 60°C for 48 h. The hardened LR White blocks were thin-sectioned at 60 nm using a microtome (Leica, Germany), and the sections were mounted on copper grids and examined by an electron microscope Themis Z (Thermo Fisher Scientific Inc., USA) at 300 kV. For bright field (BF) TEM imaging, a direct electron detection camera K2 IS (Gatan Inc., USA) was used. For high-angle annular dark field (HAADF) imaging in a scanning mode, the convergence semi-angle and collection semi-angle range were set as 18 mrad and 78–200 mrad. For energy dispersive x-ray spectroscopy (EDS) in a scanning mode, the probe current, dwell time and scan step were 1.0–1.4 nA, 50  $\mu$ s and 0.8–3.5 nm, respectively. A 3-pix average filter was used to obtain EDS net-intensity maps. BF-TEM was conducted prior to HAADF and EDS. An electron microscope JEM-ARM200F (Jeol, Japan) was also used at 80 kV for BF imaging.

### 2.3. Electrochemical Analyses

A single-chamber, three-electrode electrochemical reactor was used to investigate the EEU capability of IS5 cells in the presence or absence of FeS nanoparticles. An indium-tin-doped oxide (ITO) electrode (resistance, 5  $\Omega$ /square; thickness, 1.1 mm; surface area, 3.1 cm<sup>2</sup>) was placed at the bottom of the reactor and served as the working electrode. Ag/AgCl (saturated KCl) and Pt wire were used as the reference and counter electrodes, respectively. The electrolyte was prepared as reported previously<sup>9</sup> and contained 457 mM NaCl, 47 mM MgCl<sub>2</sub>×6H<sub>2</sub>O, 7 mM KCl, 30 mM NaHCO<sub>3</sub>, 1 mM CaCl<sub>2</sub>×2H<sub>2</sub>O, 1 mM K<sub>2</sub>HPO<sub>4</sub>, 1 mM NH<sub>4</sub>Cl, 25 mM sodium HEPES (pH 7.4), 1 mL selenite-tungstate solution, 1 mL SL-10 trace metal solution, 1 mM sodium acetate as the carbon source, and 20 mM Na<sub>2</sub>SO<sub>4</sub> as the electron acceptor. The electrolyte was sterilized by autoclaving and made anoxic by vigorous nitrogen purging. Four-day-old IS5 cells grown in DSMZ medium 195c or EASW medium were harvested by centrifugation at 7 800 × g for 10 min inside a COY anaerobic chamber under 100% N<sub>2</sub> and resuspended in 0.5 mL of the same electrolyte. Cells were introduced into each reactor to a final OD<sub>600</sub> of 0.8. Single-potential amperometry was performed at −0.4 V versus SHE. Differential pulse voltammetry (DPV) was conducted using an automatic polarization system (VMP3; Bio-Logic SAS, Paris, France) with the following parameters: pulse height, 50 mV; pulse width, 300 ms; step height, −5 mV; and step time, 2 s. The potential was scanned from positive to negative. Baseline subtraction of differential pulse (DP) voltammograms was performed using QSoas.<sup>16</sup>

### 2.4. Scanning Electron Microscopy (SEM)

After electrochemical measurements, ITO electrodes with cell attachment were immediately fixed by immersing in 2.5% glutaraldehyde prepared in phosphate buffer (0.1 M, pH 7.2) for 1 hour, under dark. After fixation, the electrodes were washed with the phosphate buffer, followed by dehydration in an ethanol gradient (25%, 50%, 75%, and 100%, 10 min each). The samples were exchanged twice in 100% ethanol, then immersed in tert-BuOH, which was

also replaced twice. The samples were frozen inside pure tert-butanol at  $-20^{\circ}\text{C}$  for 10 min then freeze-dried under a vacuum. The dried samples were coated with platinum using Quick Coater SC-701 (Sanyu Electron, Japan) and viewed with a SU5000 SEM (Hitachi High-Tech Corporation, Japan).

## 2.5. Transcriptome Analysis of IS5 under Trace- $\text{Fe}^{2+}$ and $\text{Fe}^{2+}$ -enriched Growth Conditions

IS5 cells grown for 4 days in DSMZ medium 195c or EASW were harvested by centrifugation at  $7\,800 \times g$  inside a COY anaerobic chamber. The cell pellets were immediately preserved in NucleoProtect RNA (TaKaRa Bio Inc., Japan) and processed for RNA extraction using the NucleoSpin RNA Plus kit (TaKaRa Bio Inc., Japan). Ribosomal RNA (rRNA) was removed from total RNA using the TIANSeq rRNA Depletion Kit (TIANGEN Biotech, China), and RNA-seq libraries were prepared with the Fast RNA-seq Lib Prep Kit V2 (ABclonal, USA). Sequencing was performed on a NovaSeq X Plus platform (Illumina) using 150 bp paired-end reads, generating approximately 4 Gb of data per sample. Quality-controlled reads were mapped to the draft genome of *D. ferrophilus*

IS5 using STAR<sup>17)</sup> with a minimum mapping identity of 97.53%. To compare relative expression patterns of IS5 cells under trace- $\text{Fe}^{2+}$  and  $\text{Fe}^{2+}$ -enriched growth conditions, gene expression levels were normalized as counts per million (cpm).

## 3. Results and Discussion

### 3.1. Biosynthesis of FeS Nanoparticles on the OM of IS5

To test whether IS5 biosynthesizes FeS nanoparticles on its membrane, cells were cultivated in a  $\text{Fe}^{2+}$ -enriched EASW medium containing 3.6 mM  $\text{Fe}^{2+}$ . As a control, cells were grown in the DSMZ 195c medium containing  $7.6 \mu\text{M}$   $\text{Fe}^{2+}$ . After four days, the  $\text{Fe}^{2+}$ -enriched culture had turned completely black, whereas the control remained greyish and turbid, indicating that FeS formation was strongly enhanced by elevated  $\text{Fe}^{2+}$  (Fig. S1). TEM with elemental mapping of 60-nm-thick cross-sections revealed FeS nanoparticles extracellularly, intracellularly and on the OM, with markedly larger aggregates occurring extracellularly (Figs. 1B and S2B). This size disparity is expected because  $\text{Fe}^{2+}$  and extracellular biogenic sulfide diffuse freely in the chemi-

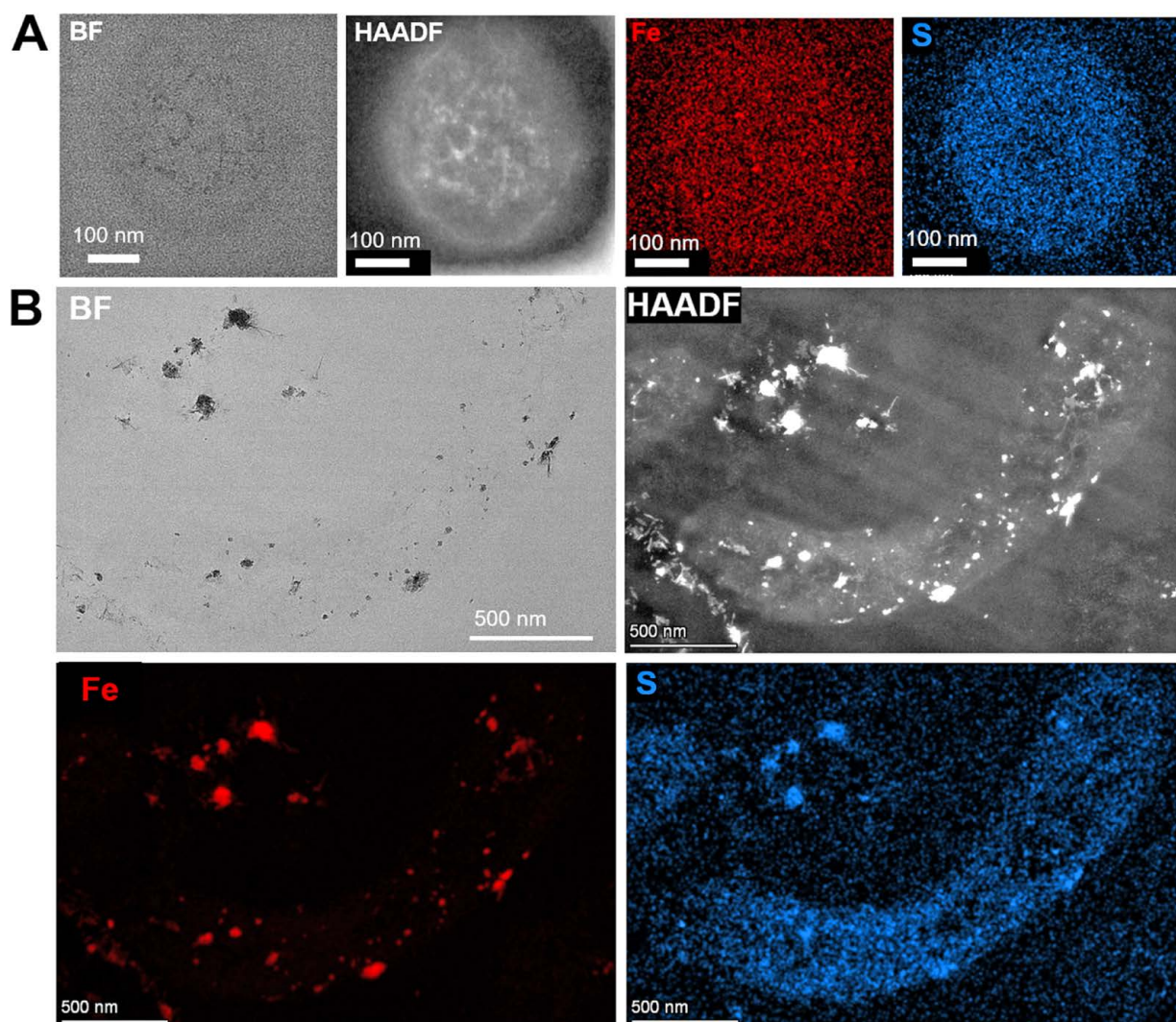


**Fig. 1.** TEM imaging of 60 nm-thick cross sections of IS5 precultivated for four days in DSMZ medium 195c containing  $7.6 \mu\text{M}$   $\text{Fe}^{2+}$  (A) or in  $\text{Fe}^{2+}$ -enriched EASW medium containing 3.6 mM  $\text{Fe}^{2+}$  (B), using BF and HAADF modes and EDS of Fe- and S-K lines. (Online version in color.)



cally unconfined extracellular medium, which promotes the formation of larger crystals. In contrast, steric confinement and limited ion mobility on the OM and within the cytoplasm—where exopolysaccharides and proteins are abundant—restrict nucleation and yield numerous smaller nanoparticles. Meanwhile, IS5 grown in DSMZ medium 195c exhibited minimal FeS biosynthesis associated with the cells (Figs. 1A and S2A). These results confirm that IS5 can biosynthesize FeS nanoparticles on its OM under elevated  $\text{Fe}^{2+}$  concentration.

### 3.2. Enhancement of EEU by Biosynthesized FeS in IS5

To assess the EEU capability of IS5 with FeS biosynthesis, cathodic current production was compared between cells precultivated in DSMZ medium and those grown in  $\text{Fe}^{2+}$ -enriched medium. After four days of cultivation, cells were harvested by centrifugation and introduced onto ITO electrodes poised at  $-0.4$  V (vs. SHE), serving as the sole electron donor. Consistent with previous studies, DSMZ-grown IS5, which depletes lactate and overexpresses OMCs,<sup>9</sup> continuously increased cathodic currents to  $-0.23 \mu\text{A cm}^{-2}$  within 20 h and maintained this level until 45 h (Fig. 2A). In contrast, IS5 containing biosynthesized FeS exhibited a more rapid and pronounced response, with currents rising to  $-0.4 \mu\text{A cm}^{-2}$  within 30 min and maintained at approximately  $-0.3 \mu\text{A cm}^{-2}$  for the next 30 h. It should be noted that the amounts of OMCs and FeS nanoparticles are unlikely to increase during the electrochemical current measurement, as IS5 remains in a non-growing and metabolically slow state when ITO electrodes are the sole electron donor.<sup>18</sup> During EEU, the trace concentration of ferrous iron in the electrolyte and the minimal sulfide production associated with this low metabolic activity would not support appreciable FeS nanoparticle synthesis. Consequently, the gradual increase in cathodic current is most likely attributed to progressive cell attachment to the electrode and physiologic adaptation toward EEU. The pronounced difference in cathodic current production indicates that IS5 precultivated under the FeS-biosynthesizing condition exhibits enhanced EEU capability.

Microscopy suggested that the enhanced EEU was due not to increased cell attachment but rather to an enhanced

EEU capacity per IS5 cell. SEM imaging of electrode surfaces showed similar cell attachment in IS5 with and without biosynthesized FeS and revealed no evidence of thick biofilm or aggregate formation induced by FeS nanoparticles (Figs. 2B, 2C). Thus, the higher current production arose from enhanced EEU capability in IS5 cells with FeS biosynthesis.

### 3.3. High-intensity Redox Signals Detected in IS5 Cells with FeS Biosynthesis

To further investigate the basis of enhanced EEU in IS5 with FeS biosynthesis, DP voltammetry was performed on cells after current production. IS5 without FeS showed a negative peak at  $-0.48$  V, attributed to OMCs,<sup>9,19</sup> whereas IS5 with biosynthesized FeS displayed a large new peak at  $-0.08$  V (previously reported for biosynthesized FeS in *D. vulgaris* Hildenborough)<sup>10</sup> and an OMC peak at  $-0.45$  V (Figs. 3A, 3B). In the DP voltammogram of IS5 with biogenic FeS (red trace in Fig. 3A), the baseline-corrected FeS peak intensity ( $\sim 280 \mu\text{A}$ ) exceeds that of the OMCs-associated peak ( $\sim 22 \mu\text{A}$ ). However, the FeS signal represents the combined contribution of extracellular and cell-surface-associated FeS in contact with the electrode and therefore cannot resolve the fraction directly involved in EEU at the cell surface. As a result, the present data do not allow a quantitative determination of whether OMCs or FeS nanoparticles constitute the dominant EEU pathway when both are present. Meanwhile, the  $\sim 30$  mV positive shift in the OMCs redox potential indicates that the heme groups in the OMCs of IS5 with biogenic FeS are slightly more oxidized, likely due to FeS-induced changes in the local electrochemical microenvironment of the hemes or weak oxidative interactions between FeS nanoparticles and the heme groups. Notably, the OMCs peak height increased nearly sixfold, suggesting that IS5 expressed more OMCs during the elevated  $\text{Fe}^{2+}$  precultivation.

### 3.4. Cytochrome Assembly Protein was Highly Upregulated during $\text{Fe}^{2+}$ -enriched Growth

We next investigated whether cells grown under  $\text{Fe}^{2+}$ -enriched conditions upregulate OMCs expression and biosynthesize FeS as an additional EEU pathway. Due to the

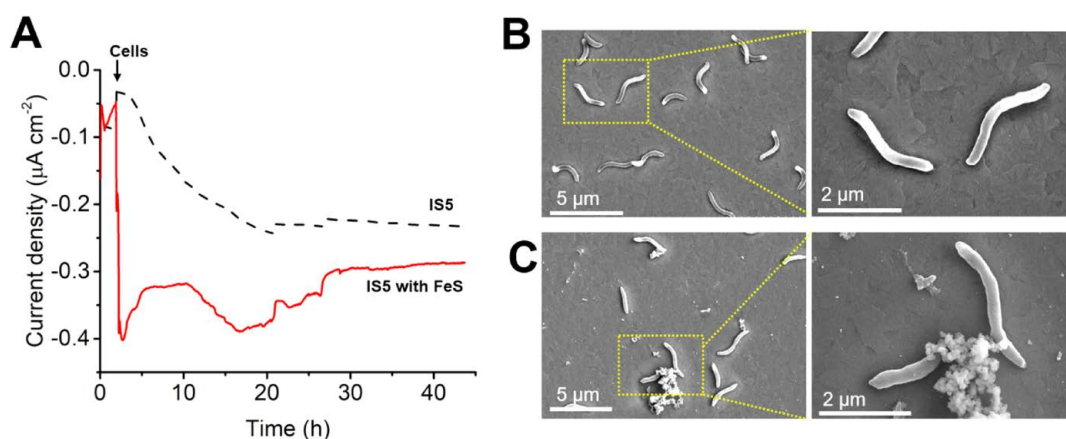


**Fig. 2.** Enhancement of cathodic current production in IS5 by FeS biosynthesis. (A) Cathodic current production by IS5 cells without or with biogenic FeS. (B, C) SEM images of electrode surfaces after electrochemical measurements with IS5 cells without (B) or with (C) biogenic FeS. (Online version in color.)

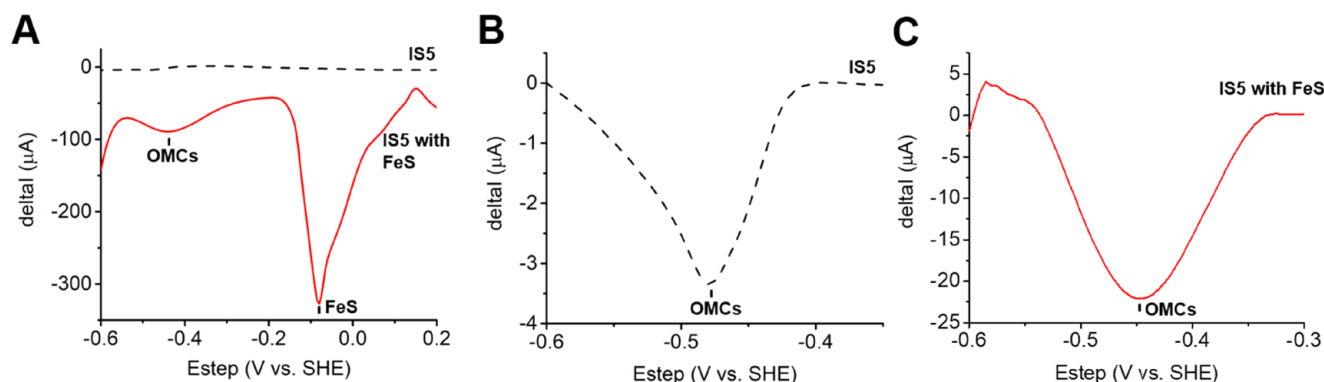


**Fig. 3.** Differential pulse (DP) voltammograms of IS5 cells, without or with biogenic FeS after current production shown in Fig. 2A. (A) DP voltammograms depicting the full scanned potential range (0.2 to  $-0.6$  V). Negative peaks assignable to FeS ( $-0.08$  V) and OMCs ( $-0.45$  V) were denoted with short bars. (B, C) Enlarged baseline-subtracted voltammograms highlighting the OMCs region. (Online version in color.)

light opacity, redox activity, and high protein adsorption affinity of FeS nanoparticles, direct OMCs quantification by UV–Vis absorption, cellular histochemical redox staining, or membrane protein analysis was not feasible. Instead, RNA expression analysis was performed for cells grown for 4 days under trace and  $\text{Fe}^{2+}$ -enriched conditions. Contrary to our expectation, genes encoding OMCs (*DFE\_448–451*, *DFE\_461–465*) showed no differential expression ( $\pm 2$ -fold). However, *DFE\_2049*, encoding a cytochrome c assembly protein for incorporating heme into apocytochrome c to form functional cytochrome c,<sup>20)</sup> was upregulated 65-fold, making it the second most up-regulated gene under the  $\text{Fe}^{2+}$ -enriched condition (Table 1). Given that the other three cytochrome c assembly genes in IS5 (*DFE\_0907*, *DFE\_1642*, and *DFE\_1646*) showed little change or only minor downregulation ( $\leq 3$ -fold), *DFE\_2049* may be preferentially employed for the maturation of OMCs, providing a possible explanation for the much stronger OMCs redox signals detected by DP voltammetry.

The other most highly upregulated genes under  $\text{Fe}^{2+}$ -enriched growth are involved in stress response, oxidative stress sensing (e.g., bacteriohemerythrin), redox balance, and unknown functions, indicating that elevated  $\text{Fe}^{2+}$  imposed significant oxidative stress on IS5, likely via Fenton-type reactions involving trace oxygen or intracellular peroxides ( $\text{Fe}^{2+} + \text{H}_2\text{O}_2 \rightarrow \text{Fe}^{3+} + \cdot\text{OH} + \text{OH}^-$ ).<sup>21)</sup> Meanwhile, the most strongly downregulated genes under  $\text{Fe}^{2+}$ -enriched growth are associated with  $\text{Fe}^{2+}$  uptake, peptide transport, and cell motility. Notably, gene clusters encoding the trans-inner-membrane redox complex HmcABCDEF (*DFE\_3360–3365*), which transfers electrons from the periplasm to cytoplasmic sulfate reduction,<sup>22)</sup> and the sulfate reduction proteins (*DFE\_2054–2056*) were significantly downregulated, suggesting that sulfate reduction is suppressed in stationary-phase cells that have accumulated abundant FeS, possibly as a strategy to prevent further FeS overproduction and cellular crowding. Additionally, the downregulation of HmcABCDEF suggests that this complex may be a significant source of oxidative species, such as superoxide, via electron leakage to trace oxygen.<sup>23)</sup>

### 3.5. FeS Nanoparticles Enable EEU in IS5 before OMCs Induction

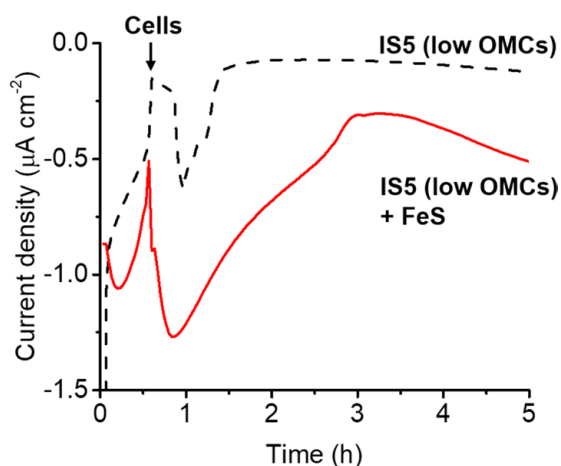
Given that biosynthesized FeS nanoparticles have been

reported as the EEU pathway in *D. vulgaris* Hildenborough,<sup>10)</sup> we tested whether they also enable EEU in IS5 that has low OMCs expression. Currently, no IS5 OMCs knockout strains exist, and the only method known to downregulate OMCs expression is to precultivate cells with excess lactate.<sup>9)</sup> Therefore, we examined the effect of increasing lactate concentration (presumably lowering OMCs expression), with or without FeS biosynthesis, by precultivating cells in modified DSMZ and EASW media containing 150 mM lactate for a shortened period of two days to prevent lactate depletion.

A much shorter timescale was used for electrochemical measurements of lactate-sufficient cells compared with lactate-starved cells (Fig. 2) to prevent OMCs production driven by stored intracellular reductive energy in an electrolyte lacking organic electron donors. Consistent with previous observations,<sup>9)</sup> IS5 cells with low OMCs produced negligible cathodic current over 5 hours, indicating that little OMCs induction occurred within this short timescale. In contrast, IS5 precultivated with excess lactate while biosynthesizing FeS was still able to increase cathodic currents (Fig. 4). Notably, because the increase in current occurred immediately after cell introduction into the reactors, FeS nanoparticles most likely enabled an acute shift from organotrophic to electrotrophic metabolism in IS5. The decrease in current between hour 1 and hour 3 following the initial increase in FeS-containing cells (red curve in Fig. 4) is attributable to cell addition during baseline stabilization, which typically requires 2–3 hours to decline to a negligible level (Fig. 2A). The current subsequently increased after hour 3, indicating that EEU-associated current production had surpassed the background current. Furthermore, lactate-excess IS5 with FeS produced a higher current than lactate-starved IS5 with FeS, as evidenced by current densities measured 4.5 h after cell addition ( $-0.55 \mu\text{A cm}^{-2}$  at hour 5 for lactate-excess cells in Fig. 4, compared with  $-0.32 \mu\text{A cm}^{-2}$  at hour 7.5 for lactate-starved cells in Fig. 2). This difference suggests that a greater number of FeS-mediated EEU pathways formed on the cell surface under the lactate-excess growth condition. This is likely attributable to reduced OMCs expression under excess lactate, which may provide more surface availability for FeS nanoparticle formation (note that the total amount of biogenic FeS was constrained by the identical  $\text{Fe}^{2+}$  con-

**Table 1.** Genes most significantly up- and downregulated under Fe<sup>2+</sup>-enriched growth. Bold text indicates gene clusters.

Gene	Product	Log <sub>2</sub> FC	Function
<i>DFE_2459</i>	universal stress protein	7.7	stress response
<i>DFE_2049</i>	cytochrome c assembly protein	6.0	heme attachment to apocytochrome c
<i>DFE_2397</i>	Nicotinamide riboside transporter PnuC	5.9	aid NAD <sup>+</sup> biosynthesis, redox balance
<i>DFE_3032</i>	hypothetical protein	5.6	
<i>DFE_2806</i>	hypothetical protein	5.4	
<i>DFE_2822</i>	bacteriohemerythrin	5.3	oxidative stress sensing
<i>DFE_0838</i>	hypothetical protein	5.3	
<i>DFE_0089</i>	hypothetical protein	5.1	
<i>DFE_2695</i>	bacteriohemerythrin	5.0	oxidative stress sensing
<i>DFE_0048</i>	universal stress protein	5.0	stress response
<b><i>DFE_1865</i></b>	<b>ferrous iron transport protein A</b>	-6.4	Fe <sup>2+</sup> uptake
<b><i>DFE_1866</i></b>	<b>ferrous iron transport protein B</b>	-6.3	
<i>DFE_0117</i>	carbon starvation protein CstA	-5.8	peptide transporter
<b><i>DFE_3360</i></b>	<b>sulfate respiration complex HmcF</b>	-4.0	Trans-inner-membrane electron transfer complex for sulfate reduction
<b><i>DFE_3361</i></b>	<b>sulfate respiration complex HmcE</b>	-5.0	
<b><i>DFE_3362</i></b>	<b>sulfate respiration complex HmcD</b>	-5.8	
<b><i>DFE_3363</i></b>	<b>sulfate respiration complex HmcC</b>	-4.7	
<b><i>DFE_3364</i></b>	<b>sulfate respiration complex HmcB</b>	-5.3	
<b><i>DFE_3365</i></b>	<b>sulfate respiration complex HmcA</b>	-5.6	
<i>DFE_3284</i>	HD-GYP domain-containing protein	-4.7	biofilm formation, motility
<i>DFE_1536</i>	ABC-type Co <sup>2+</sup> transport system, periplasmic component	-4.6	iron pool increase <sup>24)</sup>
<b><i>DFE_2054</i></b>	<b>sulfate adenylyltransferase</b>	-4.0	Converts sulfate to adenosine-5'-phosphosulfate (APS)
<b><i>DFE_2055</i></b>	<b>dissimilatory adenylylsulfate reductase beta subunit AprB</b>	-3.1	reduce APS to sulfite
<b><i>DFE_2056</i></b>	<b>adenylylsulfate reductase subunit alpha AprA</b>	-2.6	

**Fig. 4.** Enhancement of cathodic current production in IS5 with low OMCs expression by biosynthesized FeS. (Online version in color.)

centration of 3.6 mM). Together, these results indicate that FeS-biosynthesizing conditions enable IS5 to sustain EEU even under conditions of reduced OMCs expression, thereby

likely contributing to its metabolic robustness under fluctuating organic availability; however, definitive confirmation of this interpretation will require the construction and testing of IS5 OMCs knockout mutants.

#### 4. Conclusions

Our study demonstrates that cultivating IS5 under excess Fe<sup>2+</sup> substantially enhances its EEU capability. This effect arises from both increased OMCs abundance, likely mediated by upregulation of the cytochrome c assembly protein *DFE\_2049*, and the formation of additional electron uptake pathways through FeS nanoparticles. These findings provide insights into the high-rate MIC behavior of IS5: cells embedded within thick corrosion products and biofilms are likely exposed to organic limitation and elevated local Fe<sup>2+</sup> concentrations, conditions that promote both OMCs overexpression and FeS biosynthesis. These pathways may operate synergistically to enable high-rate EEU from iron and confer metabolic robustness under fluctuating organic availability.

#### Data Availability

Transcriptomic data for *D. ferrophilus* IS5 incubated

for four days in either the DSMZ medium 195c or the Fe<sup>2+</sup>-enriched EASW medium have been deposited in the NCBI GEO database under accession number GSE313310. Requests for data or information can be directed to the lead contact and will be fulfilled accordingly.

### Supporting Information

Figure S1, Figure S2, Figure S3.

This material is available on the Journal website at <https://doi.org/10.2355/isijinternational.ISIJINT-2025-353>.

### Statement for Conflict of Interest

The authors declare no conflict of interest.

### Acknowledgments

This project was financially supported by the Iron and Steel Institute of Japan (ISIJ) to X.D., and also partially supported by JAEA Nuclear Energy S&T and Human Resource Development Project Grant Number JPJA24P24021180. X.D. is grateful for the use of TEM at the Center for Basic Research on Materials and Battery Research Platform, NIMS.

### REFERENCES

- 1) B. J. Little, D. J. Blackwood, J. Hinks, F. M. Lauro, E. Marsili, A. Okamoto, S. A. Rice, S. A. Wade and H. C. Flemming: *Corros. Sci.*, **170** (2020), 108641. <https://doi.org/10.1016/j.corsci.2020.108641>
- 2) G. H. Koch, M. P. H. Brongers, N. G. Thompson, Y. P. Virmani and J. H. Payer: Cost of Corrosion in the United States, in Uhlig's Corrosion Handbook, William Andrew Publishing, Norwich, NY, (2005), 3. ISBN 9780815515005
- 3) S. E. Coetser and T. E. Cloete: *Crit. Rev. Microbiol.*, **31** (2005), 47. <https://doi.org/10.1080/10408410500304074>
- 4) D. Enning and J. Garrelfs: *Appl. Environ. Microbiol.*, **80** (2014), 1226. <https://doi.org/10.1128/AEM.02848-13>
- 5) G. Muyzer and A. J. M. Stams: *Nat. Rev. Microbiol.*, **6** (2008), 441. <https://doi.org/10.1038/nrmicro1892>
- 6) H. T. Dinh, J. Kuever, M. Mussmann, A. W. Hassel, M. Stratmann and F. Widdel: *Nature*, **427** (2004), 829. <https://doi.org/10.1038/nature02321>
- 7) D. Enning, H. Venzlaff, J. Garrelfs, H. T. Dinh, V. Meyer, K. Mayrhofer, A. W. Hassel, M. Stratmann and F. Widdel: *Environ. Microbiol.*, **14** (2012), 3073. <https://doi.org/10.1111/j.1462-2920.2012.02778.x>
- 8) M. Z. Kamil, M. Taleb-Berrouane, F. Khan and P. Amyotte: *Process Saf. Environ. Prot.*, **153** (2021), 337. <https://doi.org/10.1016/j.psep.2021.07.040>
- 9) X. Deng, N. Dohmae, K. H. Neilson, K. Hashimoto and A. Okamoto: *Sci. Adv.*, **4** (2018), eaao5682. <https://doi.org/10.1126/sciadv.aao5682>
- 10) X. Deng, N. Dohmae, A. H. Kaksonen and A. Okamoto: *Angew. Chem. Int. Ed.*, **59** (2020), 5993. <https://doi.org/10.1002/anie.201915196>
- 11) A. Picard, A. Gartman and P. R. Girguis: *Front. Earth Sci.*, **4** (2016), 68. <https://doi.org/10.3389/feart.2016.00068>
- 12) C. Zhou, R. Vannela, K. F. Hayes and B. E. Rittmann: *J. Hazard. Mater.*, **272** (2014), 16. <https://doi.org/10.1016/j.jhazmat.2014.02.046>
- 13) S. Wakai, S. Sakai, T. Nozaki, M. Watanabe and K. Takai: *Microbes Environ.*, **39** (2024), ME23089. <https://doi.org/10.1264/jsme2.ME23089>
- 14) DSMZ Medium 195c, Leibniz Institute DSMZ – German Collection of Microorganisms and Cell Cultures GmbH, “Desulfobacter sp. Medium (Lactate)”, (2022), [https://www.dsmz.de/microorganisms/medium/pdf/DSMZ\\_Medium195c.pdf](https://www.dsmz.de/microorganisms/medium/pdf/DSMZ_Medium195c.pdf), (accessed 2025-10-14).
- 15) D. Wang, P. Kijlka, M. E. Mohamed, M. A. Saleh, S. Kumseranee, S. Punpruk and T. Gu: *Bioelectrochemistry*, **142** (2021), 107920. <https://doi.org/10.1016/j.bioelechem.2021.107920>
- 16) V. Fourmond: *Anal. Chem.*, **88** (2016), 5050. <https://doi.org/10.1021/acs.analchem.6b00224>
- 17) A. Dobin, C. A. Davis, F. Schlesinger, J. Drenkow, C. Zaleski, S. Jha, P. Batut, M. Chaisson and T. R. Gingeras: *Bioinformatics*, **29** (2013), 15. <https://doi.org/10.1093/bioinformatics/bts635>
- 18) X. Deng and A. Okamoto: *Frontiers in Microbiology*, **9** (2018), 2744. <https://doi.org/10.3389/fmicb.2018.02744>
- 19) X. Deng, J. Saito, A. Kaksonen and A. Okamoto: *Environ. Int.*, **144** (2020), 106006. <https://doi.org/10.1016/j.envint.2020.106006>
- 20) D. A. I. Mavridou, S. J. Ferguson and J. M. Stevens: *IUBMB Life*, **65** (2013), 184. <https://doi.org/10.1002/iub.1123>
- 21) D. Touati: *Arch. Biochem. Biophys.*, **373** (2000), 1. <https://doi.org/10.1006/abbi.1999.1518>
- 22) A. Dolla, B. K. J. Pohorelic, J. K. Voordouw and G. Voordouw: *Arch. Microbiol.*, **174** (2000), 143. <https://doi.org/10.1007/s002030000183>
- 23) R. Z. Zhao, S. Jiang, L. Zhang and Z. B. Yu: *Int. J. Mol. Med.*, **44** (2019), 403. <https://doi.org/10.3892/ijmm.2019.4188>
- 24) P. Mihelj, I. Abreu, T. Moreyra, M. González-Guerrero and D. Raimunda: *Appl. Environ. Microbiol.*, **89** (2023), e01901-22. <https://doi.org/10.1128/aem.01901-22>